NeuroImage 311 (2025) 121206

Contents lists available at ScienceDirect

NeuroImage

journal homepage: www.elsevier.com/locate/ynimg

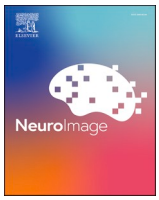

Increasing target engagement via customized electrode positioning for personalized transcranial electrical stimulation: A biophysical modeling study

Griffin Rodgers [a,b,1], Mahyar Joodaki [a,1], Alois Hopf [a,*], Emiliano Santarnecchi [c,d], Raphael Guzman [e], Bert Müller [b,f], Bekim Osmani [a,b]

[a] Bottneuro AG, Basel, Switzerland
[b] Department of Biomedical Engineering, University of Basel, Allschwil, Switzerland
[c] Precision Neuroscience and Neuromodulation Program, Gordon Center for Medical Imaging Massachusetts General Hospital, Harvard Medical School, Boston, USA
[d] Department of Neurology, Radiology & Psychiatry Massachusetts General Hospital, Boston, USA
[e] Department of Neurosurgery, University Hospital and University Children's Hospital Basel, Basel, Switzerland
[f] Department of Clinical Research, University Hospital Basel, Basel, Switzerland

ARTICLE INFO

Keywords:
Transcranial electrical stimulation
Biophysical modeling
3D-printing
Target engagement
Electrode positioning

ABSTRACT

Background: Transcranial electric stimulation (TES) is a non-invasive neuromodulation technique with therapeutic potential for diverse neurological disorders including Alzheimer's disease. Conventional TES montages with stimulation electrodes in standardized positions suffer from highly varying electric fields across subjects due to variable anatomy. Biophysical modelling using individual's brain imaging has thus become popular for montage planning but may be limited by fixed scalp electrode locations.
Objective: Here, we explore the potential benefits of flexible electrode positioning with 3D-printed neurostimulator caps.
Methods: We modeled 10 healthy subjects and simulated montages targeting the left angular gyrus, which is relevant for restoring memory functions impaired by Alzheimer's disease. Using quantitative metrics and visual inspection, we benchmark montages with flexible electrode placement against well-established montage selection approaches.
Results: Personalized montages optimized with flexible electrode positioning provided tunable intensity and control over the focality-intensity trade-off, outperforming conventional montages across the range of achievable target intensities. Compared to montages optimized on a reference model, personalized optimization significantly reduced variance of the stimulation intensity in the target. Finally, increasing available electrode positions from 32 to around 86 significantly increased target engagement across a range of target intensities and current limits.
Conclusions: In summary, we provide an *in silico* proof-of-concept that digitally designed and 3D-printed TES caps with flexible electrode positioning can increase target engagement with precise and tunable control of applied dose to a cortical target. This is of interest for stimulation of brain networks such as the default mode network with spatially proximate correlated and anti-correlated cortical nodes.

1. Introduction

Transcranial electric stimulation (TES) is a non-invasive neuromodulation technique that is extensively used to study and potentially treat a range of neurological disorders. In low-intensity TES, electric currents of up to 4 mA total and 2 mA per electrode (Antal et al., 2017) are applied via electrodes in contact with the scalp. TES is administered via an electrode montage (Bikson et al., 2019), i.e. the combination of electrode geometry, positions, and currents, which generates current flow and a related distribution of electric fields throughout the head.

* Corresponding author.
E-mail address: alois.hopf@bottneuro.ch (A. Hopf).
[1] Equal contributions.

https://doi.org/10.1016/j.neuroimage.2025.121206
Received 3 December 2024; Received in revised form 18 February 2025; Accepted 10 April 2025
Available online 12 April 2025

Variants of TES include direct current (TDCS), alternating current (TACS), and random noise stimulation (TRNS), which differ in the waveform used. Generally, TES is considered safe, with a recent analysis finding no reported serious adverse events in over 18,000 sessions (Antal et al., 2017).

There are many potential therapeutic applications of TES, each with numerous associated target regions and stimulation modalities. This leads to an enormous range of conceivable montages and metrics to summarize the dose and quality of the resulting electric field distributions (Peterchev et al., 2012). The dorsolateral prefrontal cortex has been often targeted with TDCS to improve working memory (Assecondi et al., 2021) with implications for the treatment of Alzheimer's Disease (AD) and dementia (Im et al., 2019; Rezakhani et al., 2024). Further potential target locations for AD have been identified, including cortical nodes of the default mode, memory, and attention networks, along with regions of high amyloid-β concentrations identified via PET. Specific targets include locations in the temporal lobe (Dhaynaut et al., 2022; Sprugnoli et al., 2021b), angular gyrus (Bréchet et al., 2021; Cappon et al., 2023), and precuneus (Benussi et al., 2022). Correlated and anti-correlated cortical nodes of these networks are sometimes neighboring or nearby (Briggs et al., 2018), for example the neighboring BA39 and BA7/40 regions are cortical nodes showing opposite responses to demanding cognitive tasks (Fox et al., 2005). Thus, a major challenge for TES-based therapy is precisely steering focal electric field distributions to the desired regions while avoiding off-target dose.

Due to each person's unique anatomy, the same montage results in differing electric field distributions and intensities between subjects, particularly for highly focal montages (Mikkonen et al., 2020). Inter-individual differences in cerebral spinal fluid (CSF) volume play a critical role in shaping field distributions (Kashyap et al., 2022), with sex and aging also contributing to variations (Bhattacharjee et al., 2022). This effect has been speculated to account for part of the variable subject response to TES noted in the literature, therefore a focus has been placed on accurate head modelling from subject MRIs and montage planning based on biophysical simulation (Menardi et al., 2022). Several personalized montage selection approaches based on subject-specific modelling have been presented, including various algorithms published for the optimization of electrode positions and currents to achieve a specified intensity in a target while reducing off-target stimulation (Saturnino et al., 2021; Saturnino et al., 2019c; Ruffini et al., 2014; Dmochowski et al., 2011).

Using fine electrode grids during montage optimization is a common practice to improve montage selection (Briggs et al., 2018). In real-world applications, this could be achived via fabric caps with holes for electrode positions from standardized 10–20 or 10–10 systems. An alternative approach that offers increased flexibility in electrode positioning is to produce TES caps using computer-assisted design and 3D-printing. Such an approach, shown in Fig. 1, would allow for free electrode placement within certain allowed regions. By digitally designing the cap based on a subject's head model, electrodes could be placed on a physical cap in the exact locations dictated by simulations, see Fig. 1(c). However, given the increased complexity of cap design and requirements on head modelling, the benefits of such flexible electrode placement should be quantified and compared to more well-established montage selection approaches.

In this study, we consider stimulation of a cortical target, namely the left angular gyrus (lAG), based on promising pilot studies of TES in Alzheimer's disease patients (Bréchet et al., 2021). We prepared TES montages for head models of 10 healthy subjects based on subject-specific optimization with dense, flexible electrode placement. These montages, which are inspired by 3D-printed cap manufacturing, are quantitatively compared to more traditional ad-hoc montages, montages optimized for a reference atlas model, and montages optimized based on individual head models with 32 standardized positions. Finally, we discuss how flexible electrode placement informs therapy planning and the design of future TES devices.

2. Materials and methods

2.1. Subjects

Simulations were based on MRI imaging of 10 healthy subjects. The subjects provided informed consent prior to imaging and were enrolled in the MindStim trial (NCT05999916). Two of these subjects were excluded from TES sessions by the principal investigator and thus provided no demographic information, however their MRIs were used in this simulation study as informed consent was given. For the 8 subjects with available demographic information, 5 were female and the mean age was 34 years (standard deviation 14.2 years).

2.2. MRI acquisition

T1- and T2-weighted MRIs (MPRAGE and SPACE sequences, respectively) with $1 \times 1 \times 1$ mm^3 voxel resolution were acquired using a Siemens Prisma 3T scanner (Siemens Healthcare, Erlangen, Germany) at the University Hospital of Basel (Basel, Switzerland). Field-of-view covered the entire head from cranial skin to at least C3. To minimize skin deformations, imaging was performed with minimal head constraints and patients wore earplugs rather than headphones.

2.3. Head modelling and cortical region-of-interest definition

Subject head models were created using SimNIBS' *CHARM* routine (version 4.0.1) (Puonti et al., 2020b; Thielscher et al., 2015) and

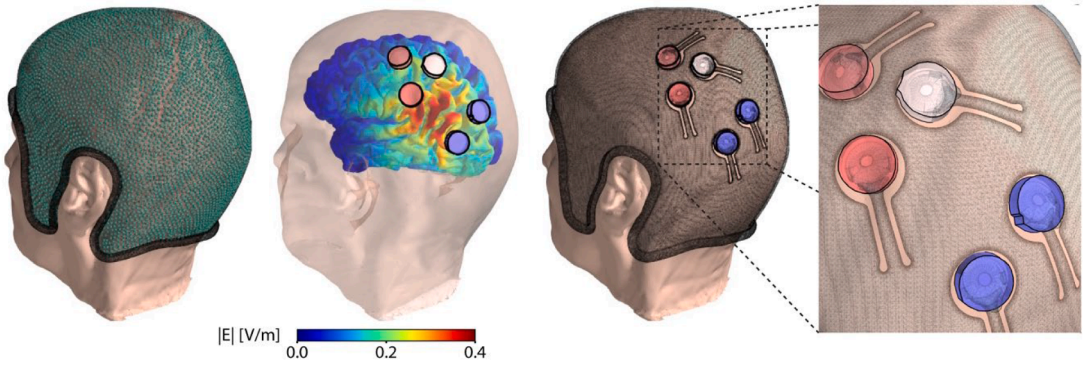

Fig. 1. Illustration of flexible electrode positioning with 3D-printed neurostimulators. Electrodes can be placed anywhere on the scalp within the cap's boundaries (a, black: cap outline, turquoise points: available positions) subject to a minimum inter-electrode spacing of 26.5 mm. Montages are selected using modelling and optimization (b), then integrated directly into the cap design file (c) for 3D-printing. This example shows a montage optimized for field magnitude of 0.3 V/m in the left angular gyrus target with current limits 1.0 mA per electrode and 2.0 mA total.

included nine components: skin, dense bone, spongy bone, cerebrospinal fluid, blood, gray matter, white matter, muscle, and eyes. Each mesh contained approximately 4.5 million elements with isotropic conductivities based on SimNIBS' standard tabulated values. Brain parcellation was performed for each subject using FreeSurfer's *recon-all* (version 7.4.1) (Fischl, 2012). We defined the lAG target based on the left parietal inferior angular gyrus from the Destrieux atlas parcellation (tag 11,125, "ctx_lh_G_pariet_inf-Angular").

2.4. Standard and custom electrode positioning systems

The standardized 10–20 system is based on an even division of the head after location of the left and right pre-auricular points, the nasion, and the inion from the subject's MRI images (Jurcak et al., 2007). SimNIBS uses a transformation from MNI space to calculate these positions, which provides reasonable accuracy (Saturnino et al., 2019b). In this study, we used a 32-electrode subset of the SPM12 10–20 extended system (see list of positions in the supplementary materials), hereafter the 32-electrode system.

We also created a custom positioning system for each subject compatible with the 3D-printed Miamind Neurostimulator (Bottneuro AG, Basel, Switzerland). For each subject, the allowed electrode positions were defined using an offset of 10 mm from the cap edges, see Fig. 1(a). For the Miamind Neurostimulator, electrodes can be freely positioned subject to a minimum inter-electrode spacing of 26.5 mm. As SimNIBS optimization does not support inter-electrode distance constraints, a subset of collision-free electrode positions was generated with a mean of 86 electrode positions. The number of electrodes in the resulting dense electrode grid varied between subjects, with more positions on larger heads. We refer to this system as the "64+" system throughout the text, as it provided >64 positions for all subjects and does not correspond to any standardized positioning system.

2.5. Electric field simulations

Electric field distributions were simulated using SimNIBS 4.0.0 (Thielscher et al., 2015). All electrodes were modelled to consist of 2 mm silicone rubber and 5 mm of saline solution.

For fixed, reference-based montages, a primary electrode at P3 was selected as this was the closest electrode from the 32-electrode system to the lAG in the reference MNI atlas. The "**conventional**" (1 × 1) montage (Bikson et al., 2019) was based on a 50 mm diameter electrode over P3 (+2 mA) and a 50 mm diameter electrode on the lower right side of the neck (−2 mA). It is more common to place a second electrode on the right shoulder in an extracephalic position, however the field of view of MRIs in this study only extended down to the C3 vertebrae. This placement impacts field distributions (Van Hoornweder et al., 2024), though the effects are more prominent in the cerebellum and spinal cord regions and are likely minor in the vicinity of the lAG target under the large P3 electrode. Further, modelling pipelines and datasets with sufficient FOV for such extended head and shoulders regions are not readily available. The "**high-definition**" montage (4 × 1) (Bikson et al., 2019; Datta et al., 2009) consisted of 18 mm diameter electrodes at P3 (+2 mA) as well as CP3, P1, P5, and PO3 (−0.5 mA each), which were adjacent to P3.

For all optimized montages, 18 mm diameter electrodes were used. Target intensities for optimization were based on studies suggesting that electric field strengths in the range of 0.2 to 0.3 V/m can affect neural activity (Liu et al., 2018; Alekseichuk et al., 2022), though it is worth noting that there are no generally agreed upon values in the community and these values are not derived from in vivo humans.

The reference-based optimization, hereafter "**MNI optimized 32″**, was performed using the 32 electrode system, the MNI152 atlas head model (provided by SimNIBS) and the lAG as a target (Saturnino et al., 2021; Saturnino et al., 2019c). To be comparable with the fixed montages, current limits were set to 2 mA per electrode and 4 mA total. The target electric field magnitude was 0.3 V/m. The optimized montage was transferred to each subject and the electric field distributions were simulated using the individual head models.

Personalized optimizations were performed using the individual head models and the lAG target. Montages were selected by optimization using both the 64+ system described above, hereafter "**optimized 64+**", and the 32-electrode system, hereafter "**optimized 32″**. Again, a target electric field magnitude of 0.3 V/m was used and current limits were set to 2 mA per electrode and 4 mA total. For the detailed comparison of personalized optimizations with 32 and 64+ systems, current limits of 1 mA and 2 mA per electrode were tested (both with 4 mA total), and target intensities of 0.1, 0.15, 0.3, and 100 V/m were used. These values represent three regimes: 0.1 or 0.15 V/m are achievable with modest current limits and allow for highly focal fields, 0.3 V/m is more realistic for therapeutic applications and is generally achievable at somewhat reduced focality, and 100 V/m, hereafter "maximum |E|", represents the maximum achievable intensity with little concern for off-target intensity.

2.6. Metrics calculation and data visualization

Simulated electric fields from all montages were interpolated onto the central gray matter surface for each subject. The quality of electric field distributions was assessed both qualitatively and quantitatively. Visual assessment was based on renderings generated with PyVista (version 0.41.1) (Sullivan and Kaszynski, 2019). Several quantitative metrics were considered: the mean electric field magnitude in the lAG, the focality of 70 % of the maximum electric field magnitude, and the correlation of the electric field magnitude with the lAG. Note that the 70 % threshold for focality is arbitrary, though it is standard in the SimNIBS library. These metrics capture complementary properties of the electric field magnitude distribution. The mean magnitude quantifies the intensity delivered to the target region but not the off-target stimulation. Focality does not consider overlap with the target or the target's relative size. Therefore, we introduced the correlation metric to capture the conformity of the field magnitude to the target. Figures S1-S4 contrast these metrics for a range of simulated montages. Increased correlation at both equal mean magnitude in target and equal focality led to visually superior field distributions. Thus, we rely on correlation instead of focality to complement the mean magnitude in target as a surrogate measure for target engagement.

3. Results

Head modelling allowed for analysis of anatomical variability of the 10 subjects. The mean (standard deviation) brain volume without ventricles and cortical volume were 1176 cm^3 (68 cm^3) and 242 cm^3 (12 cm^3), respectively. The lAG had a mean (standard deviation) surface area of 1760 mm^2 (207 mm^2) and a mean depth from the scalp surface of 21 mm (1.9 mm). The mean (standard deviation) skull thickness between scalp and lAG was 6.2 mm (1.5 mm). The location of the lAG varied with respect to the standardized 10–20 positions, which are not brain-based. The mean (standard deviation) distance from the P3 position to the nearest position on the scalp to the lAG's center-of-mass was 16.3 mm (5.3 mm). In summary, the standard deviations of these anatomical metrics are generally in the range of 10 to 30 % of the mean values.

The simulated electric field magnitude distributions for the compared montages are visualized for three subjects in Fig. 2(a), with current limits of 2 mA per electrode and 4 mA total for all montages. Column 1 shows the variation in shape and location of the lAG across the subjects. Columns 2–4 show montages designed based on the MNI head model and transferred to the subjects, with P3-centered conventional and high-definition montages as well as the "MNI optimized 32″ montage. Columns 5 and 6 show montages optimized for each subject with the 32 and 64+ systems, the latter with a mean of 86 positions.

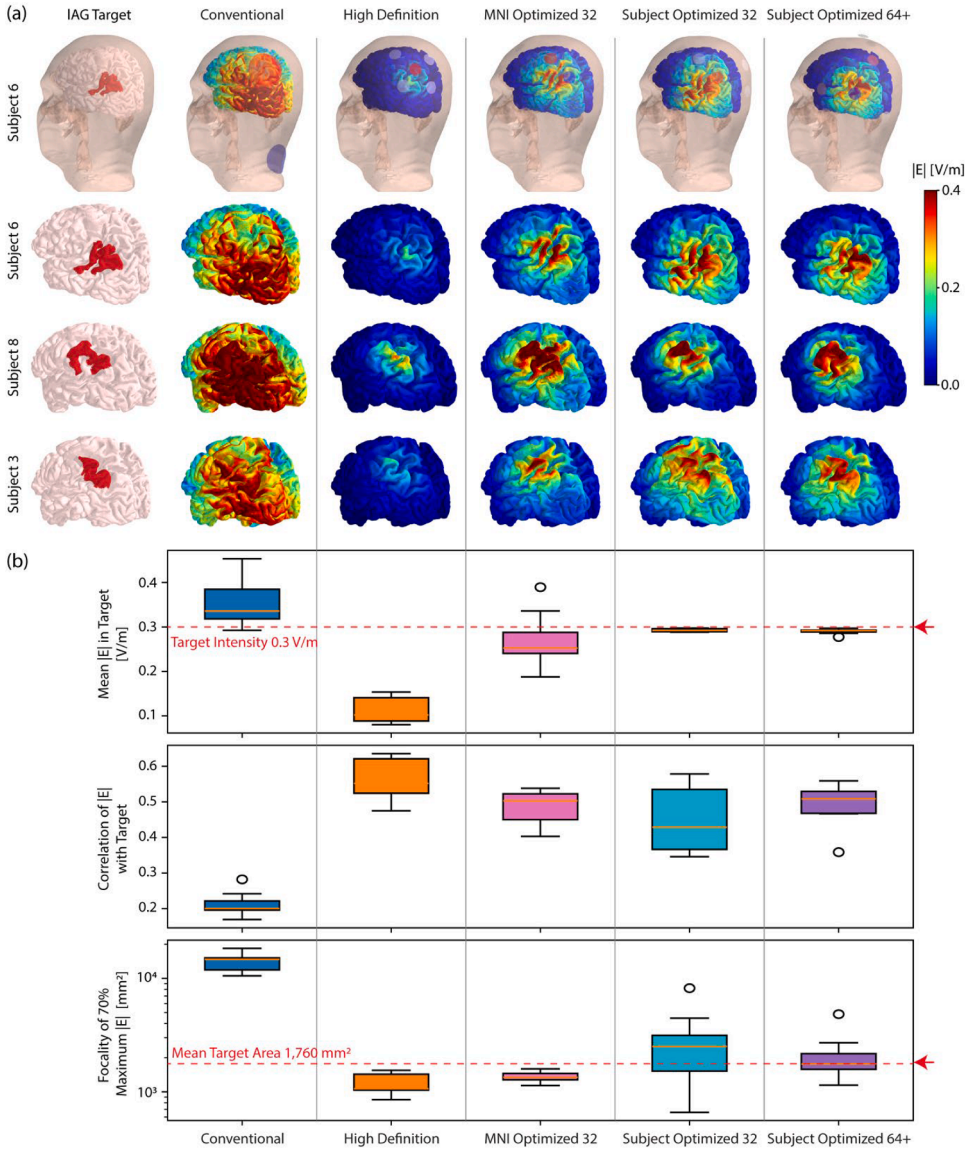

Fig. 2. (a) Electric field magnitude distributions from reference-based and personalized montages for subjects 3, 6, and 8. Montages were selected for stimulation of the lAG (column 1, red). Reference-based montages (columns 2–4) transferred standardized electrode positions from the MNI152 atlas. Personalized montages (columns 5 and 6) used subject-specific optimization. Optimization (columns 4–6) provided the best conformity of the field distribution to the target. **(b) Comparison of quantitative metrics.** Mean field magnitude in the target (top), correlation of field magnitude with target (middle), and the focality of 70 % of the maximum field magnitude (bottom) are shown for all subjects. The variance of mean field magnitude in the target (top) was significantly reduced for subject-optimized montages (Levene's test, $p < 0.05$).

Conventional montages (column 2, electrode diameter 50 mm) resulted in low focality and high intensities of >0.3 V/m across much of the left hemisphere. High-definition montages (column 3) had higher focality at lower mean intensity in the target, with observable variance in peak location and intensity. MNI optimization (column 4) resulted in less focality but higher intensities in the target compared to high-definition montages. Personalized montages (columns 5 and 6) resulted in the highest conformity of the field distribution to each subject's lAG location and morphology.

Fig. 2(b) compares the field magnitude metrics for the simulated montages with current limits of 2 mA per electrode and 4 mA total. The mean intensities in the lAG for the optimized 32 and 64+ montages were closest to the target intensity of 0.3 V/m (dashed red line in Fig. 2(b)) and had significantly reduced variance (Levene's test, $p < 0.05$) compared to all reference-based montages. The high-definition montage had the highest correlation (paired t-test, $p < 0.05$ against all others) and best focality of the montages (paired t-test, $p < 0.05$ against all except MNI optimization).

The focality of the high-definition (mean 1176 mm^2, standard deviation 261 mm^2) and MNI-optimized montages (mean 1361 mm^2, standard deviation 136 mm^2) were significantly (paired t-test, $p < 0.05$) less than that of the personalized optimized 64+ montages (mean 2119 mm^2, standard deviation 1045 mm^2). However, for stimulation of the lAG with mean surface area of 1760 mm^2 (standard deviation 207 mm^2), see dashed red line in Fig. 2(b), the more focal distributions may prove less beneficial. A complementary analysis of the Dice similarity between the peak region of the field magnitude and the target (see Figure S5) revealed greatest overlap for the subject optimized 64+ montages (paired t-test, $p < 0.1$ compared to high-definition and MNI optimized). Thus, the significant reduction in variance of the mean magnitude in target for the subject-optimized 64+ montages did not come with a meaningful loss of focality or target engagement.

Personalized optimization with both 32 and 64+ systems allowed for tunable target intensity. Fig. 3 compares conventional montages to

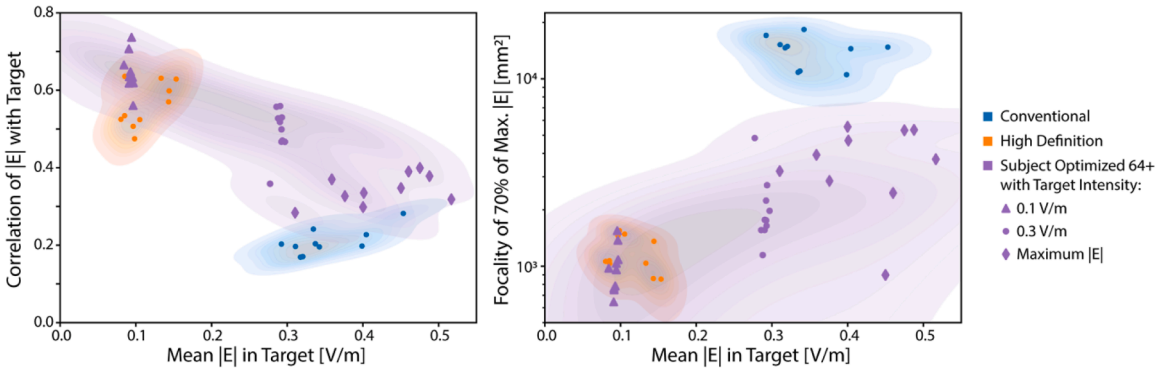

Fig. 3. Personalized optimization outperforms conventional and high-definition montages for mean intensity in target, focality, and correlation. Mean field magnitude in the lAG target is plotted against correlation of the field magnitude with the target (left) and the focality of 70 % of the maximum field magnitude (right) for conventional, high-definition, and subject 64+ optimized montages. Optimization allows for control of target intensity, therefore target intensities of 0.1, 0.3, and maximum |E| are shown. Filled contours show kernel density estimations.

personalized montages optimized over a range of target intensities using the 64+ system. These montages were all prepared with current limits of 2 mA per electrode and 4 mA total. The trade-off between intensity and correlation or focality can be seen in the inverse relationship between mean intensity and correlation (proportional for focality). The optimized 64+ montages are more pareto efficient than the fixed montages and thus outperformed traditional montages across the entire range of achievable target intensities. The inverse intensity-correlation and proportional intensity-focality relationships are explored for several current limits and finer target intensity steps Figure S6. As expected, increasing both maximum total and individual current results in more pareto efficient montages.

Fig. 4 compares optimized 32 and 64+ montages for target intensities of 0.15 V/m, 0.3 V/m, and maximum |E| as well as maximum individual currents of 1 and 2 mA. Fig. 4 (left) shows boxplots of mean magnitude in the target and correlation with the target. There were no significant differences in mean magnitude, while for all configurations the optimized 64+ montages resulted in significant increases in correlation (paired *t*-test). The mean improvement in correlation for the optimized 64+ montages was 19 %, 36 %, and 15 % for 1 mA per

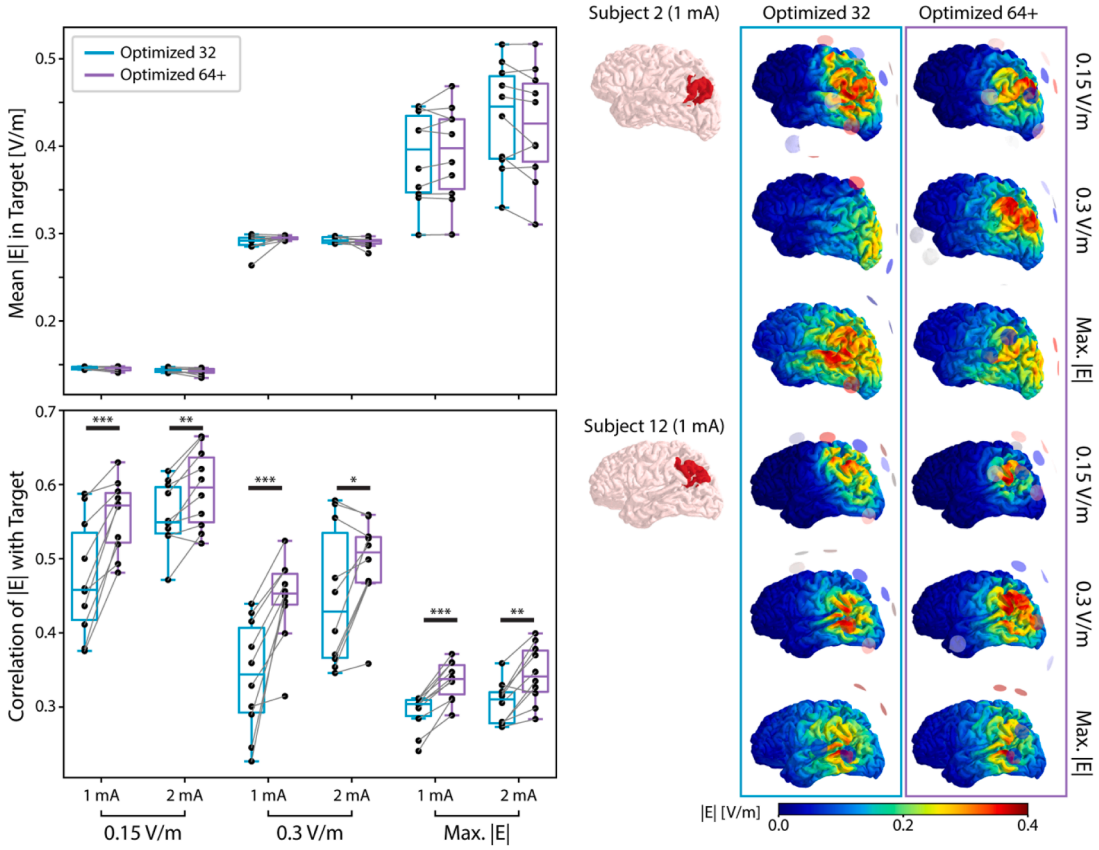

Fig. 4. Personalized optimization with more flexible electrode positioning improves correlation at equal mean intensity. Montages were prepared for all 10 subjects based on personalized optimization with 32 standardized positions and the more flexible and denser 64+ system. (Left) The mean field magnitude in the lAG as well as correlation of the field magnitude with the lAG are compared over a range of target intensities and current limits. Significance was assessed with a paired *t*-test: $*p < 0.05$, $**p < 0.01$, $*** p < 0.001$. (Right) Electric field magnitude distributions are shown for two subjects and a range of target intensities with maximum 1 mA current per electrode.

electrode and target intensities of 0.15 V/m, 0.3 V/m, and maximum |E|, respectively. The related values for 2 mA per electrode were 6 %, 13 %, and 13 %. The boxplots for focality and the Dice similarity are shown in Figure S7. The electric field magnitude distributions from the optimized 64+ montages were visually superior, see Fig. 4 (right). The improvement is especially striking for Subject 2 and target intensity of 0.3 V/m.

4. Discussion

The main findings of this simulation-based study are: (i) personalized optimization significantly reduced the variance of the mean field magnitude in the target compared to reference-based montages, i.e. fixed montages and montages optimized on the MNI atlas. (ii) Improved focality did not always correspond to improved field magnitude distributions, as focality does not directly capture the spatial position relative to the target or consider the surface area of the target region. (iii) Personalized optimization outperformed fixed montages in terms of correlation with the target and focality across all achievable target intensities. (iv) Montages from personalized optimization with the more flexible 64+ electrode system resulted in field magnitudes distributions with significantly higher correlation with the target region compared to the 32-electrode system. Result (iv) also applied for the dice similarity between 70 % of the maximum field magnitude in most scenarios and for focality in a few scenarios.

Transitioning from reference-based montages to personalized montages requires greater effort and increased costs for imaging, head modeling, and finite element method simulations. The benefit is significantly reduced variance in the mean field intensity in the target region. This is especially important as previous studies have shown traditional montages suffer from greater variability in induced electric fields as focality is increased (Mikkonen et al., 2020). Modelling-free methods for reducing intensity variance in the target region such as head circumference correction factors can somewhat reduce target intensity variance (Antonenko et al., 2021). Reverse-calculation methods use detailed 3D modelling to significantly reduce variance (Hoornweder et al., 2022; Caulfield et al., 2022; Evans et al., 2020). However, these approaches rely on personalized modelling and simulations, where montage optimization does not substantially increase workload. Further, corrected currents may exceed current limits or increase sensations, particularly in cases with a thick skull layer between electrodes and target. Most optimization strategies have the advantage that they are designed around current limits.

The strong effects of individual anatomy on field distributions shown here and in prior studies (Mikkonen et al., 2020; Bhattacharjee et al., 2022; Hoornweder et al., 2022; Mahdavi and Towhidkhah, 2018), particularly the sensitivity of field distributions to CSF volume (Kashyap et al., 2022), underscore the need for personalized modelling. Here, we have demonstrated through simulations that personalization improves electric field distributions with the hypothesis that these gains will be linked to behavioral improvements, both through increased target engagement and reduced inter-subject variability. The latter is an important aspect of reducing variability of clinical outcomes for TES-based therapies. For example, one meta-analysis revealed that montages used by most of 87 TDCS studies of working memory did not have electric field maxima in the target region (Wischnewski et al., 2021). The behavioral outcomes from ongoing and future clinical trials will surely inform the cost-benefit analysis, as the behavioral effects are the most important factor in this calculation. We note that the benefits of personalization will vary depending on the specific TES application, i.e. targeted regions and stimulation protocol. We expect our approach is more beneficial in the context of precise stimulation over longer periods with limited patient supervision, e.g. repeated at-home therapy sessions over weeks or months.

The smaller electrodes used in high-definition and optimized montages result in higher current density and thus presumably more patient sensation compared with conventional, large-electrode montages. Nevertheless, many studies have shown reasonable or good tolerability with high-definition electrodes and 1 to 2 mA currents, though individual sensations are variable and dependent on stimulation modality (Ambrus et al., 2010; Neri et al., 2020). Experiences with the Miamind Neurostimulator (Bottneuro AG, Basel, Switzerland) equipped with 18 mm diameter brush electrodes were generally favorable: all eight subjects were able to complete four 60-minute sessions receiving 40 Hz TES (maximum total current of 2 mA and maximum current per electrode of 1 mA) with this neurostimulator as part of the MindStim trial (NCT05999916) and five were willing to extend sessions beyond 60 min. Thus, the flexibility, good focality, high target engagement, and reduced variance of personalized high-definition electrodes montages should outweigh a generally manageable increase in sensation. Given the increased sensation for smaller electrodes, development of novel active-sham stimulation protocols to blind clinical trials takes on an even larger importance (Neri et al., 2020).

Increasing the number of available electrode positions during optimization clearly increased target engagement of stimulation, see Fig. 4. While both systems could provide similar intensity in target, denser positioning allowed for selection of electrodes closer to the target and thus confinement of field magnitude distribution and reduction of off-target dose. A similar effect was reported by Saturnino et al. (2019c). This advantage was larger and had greater significance when the current limit per electrode was reduced from 2 to 1 mA. Fabric EEG/TES caps can offer a variable number of potential electrode positions, for example the Neuroelectrics Starstim device (Neuroelectrics, Barcelona, Spain) offers 39- and 64-electrode position options for their 8, 20, and 32 channel devices. Incorporating digital design elements such as CAD and 3D-printing for TES devices could further increase flexibility for electrode placement, as illustrated in Fig. 1. While this paradigm allows more flexibility, here we created our 64+ system by imposing a fixed 26.5 mm inter-electrode spacing before optimization. This eliminates collisions between electrodes and their support structures, but it also drastically reduces the number of possible configurations compared to what such a device could provide. More flexibility could be achieved via heuristics or by including the distance constraint within the optimization directly. This would allow for optimization over a greater number of positions while avoiding collisions between electrodes due to hardware constrains, unlocking further improvements in target engagement. Future studies should determine how far this approach could increase target engagement, though diminishing returns are expected due to the size of electrodes, size of targets, and the electrical properties of the head itself.

The simulation methods used in this study, i.e. SimNIBS and the related libraries (Thielscher et al., 2015), have been validated in terms of segmentation accuracy (Puonti et al., 2020b) and numerical accuracy (Saturnino et al., 2019a), but only partially validated by intracranial recordings (Puonti et al., 2020a; Opitz et al., 2018), where errors are primarily expected to be the result of segmentation inaccuracies, incorrect and simplified conductivity values, and a simplified model of the contact between electrodes and scalp. Differences between virtual electrode positions on a head model and real-world positions on the subject's head also lead to deviations from expected dose, with simulation studies indicating that positional accuracy should be kept within 10 mm (Opitz et al., 2018). The general trends presented in this study are likely to persist despite increased uncertainty from these sources of error. As accuracy of personalized head modelling pipelines improve, the advantages of personalized therapy planning will likely grow.

This study is based on 10 healthy subjects from the MindStim trial (NCT05999916) for which we could ensure standardized, high quality MRI acquisition and manually check the quality of the resulting head models. While a larger sample size would be beneficial, the 10 subjects were sufficient to achieve significant reduction in dose variability through personalization (Fig. 2) as well as significant improvement of target engagement through increased flexibility in electrode placement (Figs. 4 and S7). Personalized montages outperformed traditional fixed

montages for all 10 subjects in terms of correlation of field magnitude with the lAG target at equal mean magnitude in target (Fig. 3), with kernel density estimates indicating that this trend is likely to continue in larger healthy populations. However, many therapeutic applications of TES involve individuals with brain anatomies impacted ageing (Krebs et al., 2021) and/or pathologies such as multiple sclerosis (Tecchio et al., 2022), Parkinson's disease (Manor et al., 2021), stroke (Seo et al., 2017), frontotemporal dementia (Benussi et al., 2020), AD (Im et al., 2019; Dhaynaut et al., 2022; Sprugnoli et al., 2021b; Cappon et al., 2023; Benussi et al., 2022), and gliomas (Sprugnoli et al., 2021a). In particular, brain atrophy in AD patients alters current distributions (Mahdavi and Towhidkhah, 2018), linked to the large effect of CSF volume on induced electric fields (Kashyap et al., 2022). For AD cases with atrophy and increased CSF volume, personalization using specific anatomy will likely further reducing variance compared to fixed-electrode montages or montages designed from atlases based on healthy subjects. We note that while variance will likely be reduced, the achievable target engagement in these cases may differ or be diminished compared to healthy subjects. Generation of head models in these cases is also particularly challenging, as many segmentation pipelines are mainly designed around healthy subjects and atlases. Recent developments in segmentation tools for diverse real-world imaging scenarios and anatomies (Billot et al., 2023) will aid in modelling efforts. Future studies should focus on these groups to identify if the results of this study hold.

5. Conclusion

Personalized TES montage planning significantly reduced the variance of simulated electric field magnitude in the lAG. Further, personalized optimization outperformed conventional and high-definition fixed montages in terms of both intensity and target engagement. Increasing the flexibility of electrode placement significantly improved target engagement of stimulation without changing the intensity in target. Thus, personalized montage optimization with high-density positioning systems is critical for increasing precision and reducing variance in therapeutic applications of TES. These results provide in silico validation that customized TES caps fabricated with 3D-printing can increasing target engagement for future treatment of neurological disorders including AD.

Data and code availability statement

Availability of MRI Data is restricted due to legal and ethical reasons. Access to MRI data is solely granted if data protection is guaranteed. Availability of Anaylsis codes is restricted due to the commercial nature of Bottneuro. Access to all data and code is subject to approval and a data sharing agreement between Bottneuro and the third-party. Requests to access the data should be directed to Bottneuro AG (www.bottneuro.ch, contact: mail@bottneuro.ch)

Declaration of interests

G.R., M.J., A.H., and B.O. are employees and shareholders of Bottneuro AG (Basel, Switzerland), which produces the Miamind Neurostimulator for TES therapy. E.S. is a scientific advisor for Bottneuro AG. R.G. and B.M. are shareholders of Bottneuro AG.

CRediT authorship contribution statement

Griffin Rodgers: Writing – review & editing, Writing – original draft, Visualization, Validation, Software, Methodology, Investigation, Formal analysis, Data curation, Conceptualization. **Mahyar Joodaki:** Writing – original draft, Visualization, Software, Resources, Methodology, Investigation, Formal analysis, Conceptualization. **Alois Hopf:** Writing – review & editing, Visualization, Supervision, Project administration, Methodology, Investigation, Funding acquisition, Conceptualization. **Emiliano Santarnecchi:** Writing – review & editing, Supervision. **Raphael Guzman:** Writing – review & editing, Supervision, Resources, Project administration. **Bert Müller:** Writing – review & editing, Funding acquisition. **Bekim Osmani:** Writing – review & editing, Visualization, Supervision, Project administration, Funding acquisition, Conceptualization.

Declaration of competing interest

The authors declare the following financial interests/personal relationships which may be considered as potential competing interests: Griffin Rodgers reports financial support was provided by Gebert Rüf Foundation. Griffin Rodgers reports a relationship with Bottneuro AG that includes: employment and equity or stocks. Mahyar Joodaki reports a relationship with Bottneuro AG that includes: employment and equity or stocks. Alois Hopf reports a relationship with Bottneuro AG that includes: employment and equity or stocks. Emiliano Santarnecchi reports a relationship with Bottneuro AG that includes: consulting or advisory. Raphael Guzman reports a relationship with Bottneuro AG that includes: equity or stocks. Bert Müller reports a relationship with Bottneuro AG that includes: equity or stocks. Bekim Osmani reports a relationship with Bottneuro AG that includes: board membership, employment, and equity or stocks. Mahyar Joodaki has patent #EP4204077B1 issued to Bottneuro AG. Bekim Osmani has patent #EP4204077B1 issued to Bottneuro AG. Mahyar Joodaki has patent #EP4282464B1 issued to Bottneuro AG. Bekim Osmani has patent #EP4282464B1 issued to Bottneuro AG. If there are other authors, they declare that they have no known competing financial interests or personal relationships that could have appeared to influence the work reported in this paper.

Acknowledgements

The financial support of the Gebert Rüf Foundation, Switzerland, Grant-ID GRS-058/18, is gratefully acknowledged.

Supplementary materials

Supplementary material associated with this article can be found, in the online version, at doi:10.1016/j.neuroimage.2025.121206.

Data availability

The data that has been used is confidential.

References

Alekseichuk, I., Wischnewski, M., Opitz, A., 2022. A minimum effective dose for (transcranial) alternating current stimulation. *Brain Stimul. Basic Transl. Clin. Res. Neuromodulation* 15 (5), 1221–1222. https://doi.org/10.1016/j.brs.2022.08.018.

Ambrus, G.G., Paulus, W., Antal, A., 2010. Cutaneous perception thresholds of electrical stimulation methods: comparison of tDCS and tRNS. *Clin. Neurophysiol.* 121 (11), 1908–1914. https://doi.org/10.1016/j.clinph.2010.04.020.

Antal, A., et al., 2017. Low intensity transcranial electric stimulation: safety, ethical, legal regulatory and application guidelines. *Clin. Neurophysiol.* 128 (9), 1774–1809. https://doi.org/10.1016/j.clinph.2017.06.001.

Antonenko, D., Grittner, U., Puonti, O., Flöel, A., Thielscher, A., 2021. Estimation of individually induced e-field strength during transcranial electric stimulation using the head circumference. *Brain Stimul. Basic Transl. Clin. Res. Neuromodulation* 14 (5), 1055–1058. https://doi.org/10.1016/j.brs.2021.07.001.

Assecondi, S., Hu, R., Eskes, G., Pan, X., Zhou, J., Shapiro, K., 2021. Impact of tDCS on working memory training is enhanced by strategy instructions in individuals with low working memory capacity. Sci. Rep. 11 (1), 5531. https://doi.org/10.1038/s41598-021-84298-3.

Benussi, A., et al., 2020. Transcranial stimulation in frontotemporal dementia: a randomized, double-blind, sham-controlled trial. *Alzheimers Dement. Transl. Res. Clin. Interv.* 6 (1), e12033. https://doi.org/10.1002/trc2.12033.

Benussi, A., et al., 2022. Increasing brain gamma activity improves episodic memory and restores cholinergic dysfunction in Alzheimer's disease. Ann. Neurol. 92 (2), 322–334. https://doi.org/10.1002/ana.26411.

Bhattacharjee, S., et al., 2022. Sex difference in tDCS current mediated by changes in cortical anatomy: a study across young, middle and older adults. *Brain Stimul. Basic*

Transl. Clin. Res. Neuromodulation 15 (1), 125–140. https://doi.org/10.1016/j.brs.2021.11.018.
Bikson, M., et al., 2019. Transcranial electrical stimulation nomenclature. Brain Stimulat. 12 (6), 1349–1366. https://doi.org/10.1016/j.brs.2019.07.010.
Billot, B., Magdamo, C., Cheng, Y., Arnold, S.E., Das, S., Iglesias, J.E., 2023. Robust machine learning segmentation for large-scale analysis of heterogeneous clinical brain MRI datasets. Proc. Natl. Acad. Sci. 120 (9), e2216399120. https://doi.org/10.1073/pnas.2216399120.
Bréchet, L., et al., 2021. Patient-tailored, home-based non-invasive brain stimulation for memory deficits in dementia due to Alzheimer's disease. Front. Neurol. 12. https://doi.org/10.3389/fneur.2021.598135.
Briggs, R.G., et al., 2018. A connectomic atlas of the human cerebrum—Chapter 18: the connectional anatomy of human brain networks. *Oper. Neurosurg.* 15 (suppl_1), S470. https://doi.org/10.1093/ons/opy272.
Cappon, D., et al., 2023. Tele-supervised home-based transcranial alternating current stimulation (tACS) for Alzheimer's disease: a pilot study. Front. Hum. Neurosci. 17. Accessed: Aug. 08, 2023. [Online]. Available. https://www.frontiersin.org/articles/10.3389/fnhum.2023.1168673.
Caulfield, K.A., et al., 2022. Electric field strength from prefrontal transcranial direct current stimulation determines degree of working memory response: a potential application of reverse-calculation modeling? Neuromodulation Technol. Neural Interface 25 (4), 578–587. https://doi.org/10.1111/ner.13342.
Datta, A., Bansal, V., Diaz, J., Patel, J., Reato, D., Bikson, M., 2009. Gyri-precise head model of transcranial direct current stimulation: improved spatial focality using a ring electrode versus conventional rectangular pad. Brain Stimulat. 2 (4), 201–207. e1. https://doi.org/10.1016/j.brs.2009.03.005.
Dhaynaut, M., et al., 2022. Impact of 40 hz transcranial alternating current stimulation on cerebral tau burden in patients with Alzheimer's disease: a case series. J. Alzheimers Dis. 85 (4), 1667–1676. https://doi.org/10.3233/JAD-215072.
Dmochowski, J.P., Datta, A., Bikson, M., Su, Y., Parra, L.C., 2011. Optimized multi-electrode stimulation increases focality and intensity at target. J. Neural Eng. 8 (4), 046011. https://doi.org/10.1088/1741-2560/8/4/046011.
Evans, C., Bachmann, C., Lee, J.S.A., Gregoriou, E., Ward, N., Bestmann, S., 2020. Dose-controlled tDCS reduces electric field intensity variability at a cortical target site. *Brain Stimul. Basic Transl. Clin. Res. Neuromodulation* 13 (1), 125–136. https://doi.org/10.1016/j.brs.2019.10.004.
Fischl, B., 2012. FreeSurfer. NeuroImage 62 (2), 774–781. https://doi.org/10.1016/j.neuroimage.2012.01.021.
Fox, M.D., Snyder, A.Z., Vincent, J.L., Corbetta, M., Van Essen, D.C., Raichle, M.E., 2005. The human brain is intrinsically organized into dynamic, anticorrelated functional networks. Proc. Natl. Acad. Sci. 102 (27), 9673–9678. https://doi.org/10.1073/pnas.0504136102.
Hoornweder, S.V., Caulfield, K.A., Nitsche, M., Thielscher, A., Meesen, R.L.J., 2022. Addressing transcranial electrical stimulation variability through prospective individualized dosing of electric field strength in 300 participants across two samples: the 2-SPED approach. J. Neural Eng. 19 (5), 056045. https://doi.org/10.1088/1741-2552/ac9a78.
Im, J.J., et al., 2019. Effects of 6-month at-home transcranial direct current stimulation on cognition and cerebral glucose metabolism in Alzheimer's disease. *Brain Stimul. Basic Transl. Clin. Res. Neuromodulation* 12 (5), 1222–1228. https://doi.org/10.1016/j.brs.2019.06.003.
Jurcak, V., Tsuzuki, D., Dan, I., 2007. 10/20, 10/10, and 10/5 systems revisited: their validity as relative head-surface-based positioning systems. NeuroImage 34 (4), 1600–1611. https://doi.org/10.1016/j.neuroimage.2006.09.024.
Kashyap, R., et al., 2022. Variation of cerebrospinal fluid in specific regions regulates focality in transcranial direct current stimulation. Front. Hum. Neurosci. 16. https://doi.org/10.3389/fnhum.2022.952602.
Krebs, C., Peter, J., Wyss, P., Brem, A.-K., Klöppel, S., 2021. Transcranial electrical stimulation improves cognitive training effects in healthy elderly adults with low cognitive performance. *Clin. Neurophysiol.* 132 (6), 1254–1263. https://doi.org/10.1016/j.clinph.2021.01.034.
Liu, A., et al., 2018. Immediate neurophysiological effects of transcranial electrical stimulation. Nat. Commun. 9 (1), 5092. https://doi.org/10.1038/s41467-018-07233-7.
Mahdavi, S., Towhidkhah, F., 2018. Computational human head models of tDCS: influence of brain atrophy on current density distribution. *Brain Stimul. Basic Transl. Clin. Res. Neuromodulation* 11 (1), 104–107. https://doi.org/10.1016/j.brs.2017.09.013.
Manor, B., et al., 2021. Multitarget transcranial electrical stimulation for freezing of gait: a randomized controlled trial. *Mov. Disord.* 36 (11), 2693–2698. https://doi.org/10.1002/mds.28759.
Menardi, A., et al., 2022. Toward noninvasive brain stimulation 2.0 in Alzheimer's disease. Ageing Res. Rev. 75, 101555. https://doi.org/10.1016/j.arr.2021.101555.
Mikkonen, M., Laakso, I., Tanaka, S., Hirata, A., 2020. Cost of focality in TDCS: interindividual variability in electric fields. *Brain Stimul. Basic Transl. Clin. Res. Neuromodulation* 13 (1), 117–124. https://doi.org/10.1016/j.brs.2019.09.017.
Neri, F., et al., 2020. A novel tDCS sham approach based on model-driven controlled shunting. Brain Stimulat. 13 (2), 507–516. https://doi.org/10.1016/j.brs.2019.11.004.
Opitz, A., Yeagle, E., Thielscher, A., Schroeder, C., Mehta, A.D., Milham, M.P., 2018. On the importance of precise electrode placement for targeted transcranial electric stimulation. NeuroImage 181, 560–567. https://doi.org/10.1016/j.neuroimage.2018.07.027.
Peterchev, A.V., et al., 2012. Fundamentals of transcranial electric and magnetic stimulation dose: definition, selection, and reporting practices. Brain Stimulat. 5 (4), 435–453. https://doi.org/10.1016/j.brs.2011.10.001.
Puonti, O., Saturnino, G.B., Madsen, K.H., Thielscher, A., 2020a. Value and limitations of intracranial recordings for validating electric field modeling for transcranial brain stimulation. NeuroImage 208, 116431. https://doi.org/10.1016/j.neuroimage.2019.116431.
Puonti, O., Van Leemput, K., Saturnino, G.B., Siebner, H.R., Madsen, K.H., Thielscher, A., 2020b. Accurate and robust whole-head segmentation from magnetic resonance images for individualized head modeling. NeuroImage 219, 117044. https://doi.org/10.1016/j.neuroimage.2020.117044.
Rezakhani, S., Amiri, M., Hassani, A., Esmaeilpour, K., Sheibani, V., 2024. Anodal HD-tDCS on the dominant anterior temporal lobe and dorsolateral prefrontal cortex: clinical results in patients with mild cognitive impairment. Alzheimers Res. Ther. 16 (1), 27. https://doi.org/10.1186/s13195-023-01370-y.
Ruffini, G., Fox, M.D., Ripolles, O., Miranda, P.C., Pascual-Leone, A., 2014. Optimization of multifocal transcranial current stimulation for weighted cortical pattern targeting from realistic modeling of electric fields. NeuroImage 89, 216–225. https://doi.org/10.1016/j.neuroimage.2013.12.002.
Saturnino, G.B., Madsen, K.H., Thielscher, A., 2019a. Electric field simulations for transcranial brain stimulation using FEM: an efficient implementation and error analysis. J. Neural Eng. 16 (6), 066032. https://doi.org/10.1088/1741-2552/ab41ba.
Saturnino, G.B., Madsen, K.H., Thielscher, A., 2021. Optimizing the electric field strength in multiple targets for multichannel transcranial electric stimulation. J. Neural Eng. 18 (1), 014001. https://doi.org/10.1088/1741-2552/abca15.
Saturnino, G.B., Puonti, O., Nielsen, J.D., Antonenko, D., Madsen, K.H., Thielscher, A., 2019b. SimNIBS 2.1: a comprehensive pipeline for individualized electric field modelling for transcranial brain stimulation. In: Makarov, S., Horner, M., Noetscher, G. (Eds.), Brain and Human Body Modeling: Computational Human Modeling at EMBC 2018. Springer International Publishing, Cham, pp. 3–25. https://doi.org/10.1007/978-3-030-21293-3_1.
Saturnino, G.B., Siebner, H.R., Thielscher, A., Madsen, K.H., 2019c. Accessibility of cortical regions to focal TES: dependence on spatial position, safety, and practical constraints. NeuroImage 203, 116183. https://doi.org/10.1016/j.neuroimage.2019.116183.
Seo, H.G., Lee, W.H., Lee, S.H., Yi, Y., Kim, K.D., Oh, B.-M., 2017. Robotic-assisted gait training combined with transcranial direct current stimulation in chronic stroke patients: a pilot double-blind, randomized controlled trial. *Restor. Neurol. Neurosci.* 35 (5), 527–536. https://doi.org/10.3233/RNN-170745.
Sprugnoli, G., et al., 2021a. Personalised, image-guided, noninvasive brain stimulation in gliomas: rationale, challenges and opportunities. EBioMedicine 70, 103514. https://doi.org/10.1016/j.ebiom.2021.103514.
Sprugnoli, G., et al., 2021b. Impact of multisession 40Hz tACS on hippocampal perfusion in patients with Alzheimer's disease. Alzheimers Res. Ther. 13 (1), 203. https://doi.org/10.1186/s13195-021-00922-4.
Sullivan, C.B., Kaszynski, A.A., 2019. PyVista: 3D plotting and mesh analysis through a streamlined interface for the Visualization Toolkit (VTK). J. Open Source Softw. 4 (37), 1450. https://doi.org/10.21105/joss.01450.
Tecchio, F., et al., 2022. Home treatment against fatigue in multiple sclerosis by a personalized, bilateral whole-body somatosensory cortex stimulation. *Mult. Scler. Relat. Disord.* 63, 103813. https://doi.org/10.1016/j.msard.2022.103813.
Thielscher, A., Antunes, A., Saturnino, G.B., 2015. Field modeling for transcranial magnetic stimulation: a useful tool to understand the physiological effects of TMS?. In: 2015 37th Annual International Conference of the IEEE Engineering in Medicine and Biology Society (EMBC), pp. 222–225. https://doi.org/10.1109/EMBC.2015.7318340.
Van Hoornweder, S., et al., 2024. Head and shoulders—The impact of an extended head model on the simulation and optimization of transcranial electric stimulation. Imaging Neurosci. 2, 1–11. https://doi.org/10.1162/imag_a_00379.
Wischnewski, M., Mantell, K.E., Opitz, A., 2021. Identifying regions in prefrontal cortex related to working memory improvement: a novel meta-analytic method using electric field modeling. *Neurosci. Biobehav. Rev* 130, 147–161. https://doi.org/10.1016/j.neubiorev.2021.08.017.